Microscopical observations of interface cracks from inter-fibre failure under compression in composite laminates

Patricia Lucía Zumaquero, Elena Correa*, Jesús Justo, Federico París

Departamento de Mecánica de Medios Continuos y Teoría de Estructuras, Grupo de Elasticidad y Resistencia de Materiales, Escuela Técnica Superior de Ingeniería, Universidad de Sevilla, Sevilla, España.

*Corresponding author: ecorrea@us.es

Camino de los Descubrimientos s/n, Escuela Técnica Superior de Ingeniería, 41092, Sevilla, España

Abstract

Matrix/Inter-fibre failure is characterized by the appearance at the fibre-matrix interfaces of small debonds that can progress along them until reaching a certain extension, then changing their orientation to kink towards the matrix and, finally, growing through it. The particular case of compressive loading is specially interesting, given the morphology of the interface cracks and the specific angle that the macro-cracks form in the matrix.

To date, the analysis of this problem at micro-mechanical level has been carried out mainly by means of Finite Element or Boundary Element models. In this work, the problem is approached from the experimental point of view, observing under optical microscope those coupons previously tested at different loading levels. Several aspects such as the identification of the stages of the failure mechanism, the kinking angle, the extension of the interface cracks and the presence of damage as a function of the loading level are studied.

Keywords: B. Debonding; B. Transverse cracking; C. Micro-mechanics; D. Optical microscopy.

1. Introduction

The study of the initiation of failure mechanisms in composite materials at micro-mechanical level is essential for the improvement of the existing criteria that predicts their appearance; the connection of the knowledge generated at this level with the macro-mechanical scale would contribute to a more accurate and efficient design of components made of composites.

The particular case of matrix/inter-fibre failure under compression, which corresponds, at the macro-mechanical level, to transverse failure under compression (i.e. failure occurring in 90º plies of multidirectional laminates or in unidirectional laminates subjected to transverse loads) has been analysed by several authors using numerical tools, see for instance Correa et al. [1-4], González and Llorca [5], Vaughan and McCarthy [6], Yang et al. [7] and Arteiro et al. [8]. In particular, the work by Correa et al. [1-4] identified the initial stages of the damage mechanism, and showed the importance of some key parameters on the progression of damage.

Specifically, as Figure 1 shows, the damage is assumed to initiate at the fibre-matrix interfaces as small (10º length) debonds (interface cracks) centred at 135º; these initial debonds (Stage I, Figure 1a) present an interesting morphology characterized by an almost closed (contact) configuration with a small 'bubble' in their lower tip [1]. The debond growth along the interface (Stage II, Figure 1b) seems to be unstable until reaching a certain extension at the interface that coincides with the closing of the

‘bubble’; this final amplitude of the crack at the interface is approximately 76º (corresponding to a position of the lower crack tip of 206º).

After this moment, the interface crack growth turns stable, giving rise to Stage III of the damage mechanism, i.e. the kinking of the crack towards the matrix (Figure 1c). A very remarkable feature is that the crack does not kink into the matrix following an arbitrary orientation but an approximate angle of 53º with reference to the external load, coinciding with the macro-mechanical fracture angle detected experimentally (Figure 1d) and presumably formed by the coalescence of the aforementioned kinked cracks (named as Stage IV). This characteristic macro-mechanical failure angle has already been brought to light by other authors (see for instance Puck and Schürmann [9] and Christensen and De Teresa [10]).

Previous works from different authors focusing on the experimental micro-mechanical observation of the matrix failure can be found in the literature, see for instance Zhang et al. [11], Gamstedt and Sjögren [12], Saito et al. [13], Baral et al. [14], Hobbiebrunken et al. [15], or Genz et al. [16], although micro-mechanical experimental investigations specifically devoted to transverse compression are not easily found.

Based on the numerical studies performed by Correa et al. [1-4] on the behaviour of composites subjected to compressive transverse loads, this work focuses on the experimental identification of the different stages of the damage mechanism arising in coupons from 90º unidirectional and symmetrical cross-ply laminates subjected to compression.

Thus, in this study, the following four stages of the damage mechanism will be experimentally distinguished:

- Stage I: Damage initiation at the interface.
- Stage II: Interface crack growth.
- Stage III: Interface crack kinking towards the matrix.
- Stage IV: Formation of a macro-crack.

The approach conceived for the investigation presented here has consisted on the manufacturing of coupons of two different types (unidirectional and cross-ply) (Section 2.1), their testing under compression at different loading levels lower than the strength of the corresponding laminates (Section 2.2), the preparation of samples (Section 3), and their inspection by means of an optical microscope (Section 4), analyzing the damage encountered and searching for an experimental base to validate the predictions of the previous numerical models. Specifically, key aspects of the stages such as the extension of Stage I debonds (Section 4.3), the amplitude of the interface crack that gives rise to Stage III (Section 4.4) and the kinking angle (Section 4.5) are studied.

2. Coupons manufacturing and testing

2.1 Coupons manufacturing

The coupons for compressive tests (Figure 2) were manufactured based on ASTM D695-02a [17] and using a carbon/epoxy (*Hexply AS4/8552)* pre-preg. This material contains a 34% resin content and 194g of fibre per unit area. The corresponding reinforcing tabs were bonded using a standard epoxy film adhesive with a polyamide base (*AF-163-2-K.06)* from 3M.

Two different sets of coupons were manufactured: a first set from unidirectional 90º panels with 10 plies (and using the same laminate to build the tabs), Figure 3a; a

second set from cross-ply symmetrical panels $[0_3, 90_3]_s$ with tabs from a $[0_{12}]$ laminate, Figure 3b. Coupons tested at different loading levels belong to different panels.

2.2. Transverse compressive tests

Transverse compressive tests were performed using the set-up presented in Figure 4.

2.2.1. Unidirectional coupons

A first set of 5 unidirectional (UD) coupons was selected for testing under compression. The results obtained for the compressive strength (Y_c) showed a mean value of 279.8 MPa, a standard deviation of 4.8 MPa and a coefficient of variation of 1.7%, therefore implying an excellent result in terms of dispersion.

Subsequent testing campaigns were performed under maximum loads lower than the previously measured Y_c, in order to generate damage without reaching the catastrophic failure. In particular, the loads applied can be grouped in 4 levels: 25%Y_c, 50%Y_c, 75%Y_c and 80%Y_c, using 6 coupons for each group. The reason for the selection of these specific loading levels will be explained in Section 4.1.

2.2.2. Cross-ply coupons

A similar procedure was employed in this case. A first set of 5 coupons was selected for testing under compression. The results obtained for the compressive strength of the laminate (X) showed a mean value of 883.7 MPa, a standard deviation of 23.9 MPa and a coefficient of variation of 2.7%, again implying and excellent result in terms of dispersion.

Subsequent testing campaigns were performed under maximum loads lower than the previously measured X, aiming to generate damage at the 90º layer without reaching the catastrophic failure of the whole laminate. In particular, the loads applied can be grouped in 4 levels: 70%X (1 coupon), 75%X (6 coupons), 90%X (6 coupons) and 95%X (5 coupons). The reason for the selection of these specific loading levels and number of coupons will be explained in Section 4.1.

3. Samples preparation for microscopical observation

The samples preparation for optical inspection consists of two phases. In the first one the coupon must be encapsulated. To this end, the coupon is cut using a diamond disc saw and is introduced in a 40 mm diameter polypropylene mould with removable base; acrylic resin for cold inlay (obtained from the mixture of *VersoCit-2 Powder* and *VersoCit-2 Liquit kits*) is poured into the mould and cured at room temperature. The second phase consists of the sanding and polishing of the samples after removing them from their moulds; a Saphir 520 polisher from NEURTEK Instruments and a LaboDoser liquide dispenser from STRUERS were used in this case.

As explained in Correa et al. [18], the result of the polishing process must allow the fibres corresponding to the 90º plies to be clearly observed in an optical microscope at 1000x magnification. The detail of the four steps of the polishing process specially designed for this case is described in Table 1, whereas Figure 5 contains, as an example, an image of the third step.

Finally, the polished samples were washed in order to remove any remains and carefully dried avoiding damage to the surfaces ready for inspection. An image of the

final state of the resulting samples is presented in Figure 6, showing the quality required to obtain good observations.

4. Microscopical observation

The microscopical observation has been made using an optical microscope *Eclipse MA100* from Nikon and *Perfect Image V8.01* software for the acquisition and edition of pictures.

4.1. Macro-cracks

4.1.1. Unidirectional coupons

A first inspection of the transverse unidirectional coupons from groups 25%Y_c, 50%Y_c, and 75%Y_c and those tested to failure showed that macro-cracks visible at low magnification (25x) appeared only in the last group (coupons tested to failure), due to a sudden and catastrophic failure mechanism. This conclusion is supported by the observations made during the compressive transverse tests; in particular, no visible damage or audible acoustic emission was detected during the tests before any coupon breakage and no non-linearity appeared in the load displacement curves before ultimate failure.

The 80%Y_c group was then tested and inspected at low magnification but no macro-cracks were found either. The same procedure was attempted with additional coupons at 85%Y_c and 90%Y_c but led to premature failure. Macro-cracks visible at high magnification (1000x) (which are considered here as Stage IV of the mechanism of damage, see Section 1), were detected in coupons tested at 50%Y_c and 80%Y_c.

4.1.2. Cross-ply coupons

Based on Correa et al. [18] these coupons were initially conceived as an alternative to the transverse unidirectional ones expecting to find macro-cracks visible when using low magnification at loading levels lower than that leading to the final breakage. As no macro-cracks where found at 70%X level, the inspection was concentrated in loads greater than this one. Notice that, using CLT theory, 70%X would correspond to a stress at the 90º layer lower than Y_c, which supports the absence of macro-cracks at this loading level.

The microscopical observation revealed again that only coupons tested until breakage showed macro-cracks visible at low magnification. At loading levels close to the laminate strength (90%X and 95%X) some macro-cracks were detected at high magnification.

4.2. Initial stages and other damage observed

As explained in Section 1, taking the numerical predictions from Correa et al. [1-4] as a reference, the different stages of the mechanism of damage need to be microscopically identified.

First of all, it is important to highlight that the three initial stages (Figure 1) were observed at all loading levels lower than Y_c in the unidirectional coupons, but they were more difficult to identify in the cross-ply coupons, where, for instance, Stage I was only detectable at 95%X. Figure 7 contains an example of each stage.

In addition to the stages predicted by the previous numerical studies, other types of damage were detected in both unidirectional and cross-ply coupons (notice that the numbering continues the list started by the Stages I to IV and thus begins at V):

- Damage V: Hole in the matrix (Figure 8a).
- Damage VI: Crack tangent to one or several fibres (Figure 8b).
- Damage VII: Crack touching a point of a fibre (Figure 8c).
- Damage VIII: Crack in the matrix (Figure 8d).

None of these types of damage were observed in the previous inspection of two untested specimens, in agreement with the study presented in Correa et al [18]. Anyhow, Damage V could have its origin in a matrix void, originated during the manufacturing process.

4.2.1. Unidirectional coupons

In the case of unidirectional coupons, the total number of imperfections (Stages I to IV and other types of Damage, V to VIII) encountered at each loading level is registered in Table 2, showing the detail and significance of the observations made. In Table 3 the type of imperfection and its percentage of appearance for each loading level are detailed. In particular, Table 2 shows the total number of imperfections without specifying the type of damage encountered. Table 3 provides this additional information. The percentage of appearance of each type of damage at the different loading levels gives information about how evolved the damage mechanism is (for instance, from Table 3 it is deduce that Stage I decreases its presence as the loading level increases) and how relevant the other types of damage are (in principle not directly

connected with the damage mechanism explored) and if they have a clear connection with the loading level.

The information presented in Table 3 leads to the conclusion that the types of Damage VI, VII and VIII prevail at all loading levels. In contrast (and as mentioned in the previous Section) Stage IV is only present in coupons tested at $50\%Y_c$ and $80\%Y_c$. The remaining stages are localized at all loading levels.

Additionally, two isolated examples of very large debonds have been detected close to a macro-crack in two coupons tested to failure; a picture of one of them is presented in Figure 9. The appearance of this type of debonds has been studied in more detail by Correa et al [18], where microscopical observations of coupons tested under transverse tension were presented.

4.2.2. Cross-ply coupons

Table 4 shows the total number of imperfections counted at each loading level of cross-ply coupons, whereas Table 5 completes this information adding the occurrence of each imperfection (in percentage). As happened with Tables 2 and 3, Table 4 shows the total number of imperfections but without specifying the type of damage encountered. Table 5 provides this additional information.

Notice that a second column for 95%X appears in Table 5 (95%X (b)), corresponding to the inspection in some coupons after a second polishing process once the first one was considered to be insufficient (showing some polishing marks and remains).

As can be observed in Table 5, at all loading levels the types of Damage VI and VIII prevail. In contrast, Stage I is only present at 95%X and after the second polishing process (95%X (b)), where a greater number of imperfections were counted. Although this increase in the number of imperfections could be a foreseeable result, the effect of subsequent polishing processes on the microscopical inspection is an interesting issue to be studied, since aspects such as the length of the cracks in the longitudinal direction could affect the results. A different observer following the same procedure should obtain similar results. Nevertheless, the numbers could change with the coupon due to the dispersion in the strength determination. It could also change with the location of the plane observed.

Finally, from the comparison of unidirectional and cross-ply samples it is concluded that Stage I is more frequently observed and at lower loading levels in the unidirectional coupons. Stage IV is more common in cross-ply coupons, a fact that may be associated with the constraining effect of the 0º layer, which may allow the generation of a greater number of macro-cracks in the 90º layer before the complete failure of the coupon. Conversely, in unidirectional coupons failure occurs due to unstable propagation of one of these macro-cracks quickly after their formation.

4.3 Stage I identification

The localization of the initiation of damage at the fibre-matrix interfaces in the different samples, i.e. Stage I, helps to establish the loading level associated with damage nucleation.

As it has been mentioned in Section 4.2, in the case of unidirectional laminates, Stage I is found (although not profusely) at all loading levels; in the case of cross-ply laminates it is only detected at 95%X. This could be due to the fact that the 90º layer thickness of the unidirectional coupons is greater than the cross-ply one, increasing the observation area, and consequently the probability of finding damage nucleation sites (Stage I). In addition, because the inter-fibre failure under compression is quite unstable, Stage I would rapidly change to Stage II and even Stage III, making its detection quite difficult in both cases but specially in the cross-ply coupons (as was already pointed out in the previous section). In-situ observations could be an appropriate alternative to overcome this difficulty.

Previous numerical works assumed 10º as the extension of the debonds associated with Stage I [1]. This was based on stress/strength concepts, i.e. on the fact that shear stresses were constant along such arc-length. Yet, no debonds lower than 20º have been found in the present investigation, therefore the decision has been to classify as Stage I those debonds whose length is in the range of 20º-30º. Figure 10, corresponding to a unidirectional coupon tested under 25%Y_c, shows an example of a Stage I debond, detailing its specific angular extension (belonging to the aforementioned range); it can be checked that this debond is centred at ~40º, in good agreement with the numerical predictions [1], that fixed it a 45º.

Notice that these larger values of Stage I debonds experimentally detected are in better agreement with the more recent predictions on this subject made under the light of Finite Fracture Mechanics (Mantič [19], Mantič and García [20]), which combine stress and energy concepts. This paper follows the approach of the previous numerical studies by the authors where the separation between Stages I and II is considered. It was

not clear, in advance, if the separation between both Stages was real or not. After the experimental tests this fact is still unclear as the tools employed seem to be insufficient for its detection, although a smallest size of the debond at the interface has been found. In-situ observations and electronic microscopy seem suitable alternatives for a deeper study of this question. The unstable character of the failure mechanism and the dependence of the initiation of failure on the properties of the interface (in particular on the fracture toughness) are some of the features that make it an open question.

4.4. Measurement of Stage II debond extension

Another interesting point of study is the measurement of the final extension of the crack at the interface (Stage II) that gives rise to Stage III (represented by the debonding angle θ_d in Figure 1).

These measurements have been carried out on macro-cracks visible at low magnification, in particular in those samples from coupons tested until breakage.

The criterion employed for the measurement has consisted on the consideration of the fibre that housed the debond as a single one, linking the total length of the crack to that fibre without considering its possible sharing with the nearby ones. This is especially relevant in the cases where, due to the proximity between fibres, it is not possible to distinguish the exact point at a fibre interface where the crack joined the interface crack coming from another fibre. This problem would not arise in the case of isolated fibres.

Although being an acceptable criterion, it is true that it can lead to measures greater than the real values. To explain this fact, Figure 11 presents an example: it has

been plotted in white colour the angular measurement using this criterion (82º) and, in black, the extension of the debond just measuring the portion between the line joining the centres of the fibres that share the debond (in grey) and the final position of the crack in the considered fibre (~63º). An approximate difference of 19º exists between both measures in this particular example. A deeper analysis of the measured debonds leads to a maximum difference between both criteria of 25.6º. In spite of this fact, the aforementioned criterion was used in all measurements performed (isolated and non-isolated fibres) as it allows the joint treatment of all cases; however, its discussed inconveniences are taken into account when deriving conclusions from the results obtained.

Focusing now on the results of the measurement of the final extension of the debonds at the interface for both types of coupons, 322 is the number of θ_d measurements performed in the group of samples corresponding to the unidirectional laminate, whereas 281 is the number associated with the cross-ply laminate, showing the statistical relevance of the study performed. Notice that no immediate explanation can be found for the difference observed in the numbers associated with each type of coupon, due to the fact that they show different sizes of the inspection area (10 plies in the unidirectional type and 6 plies in the cross-ply one), they are subjected to different loading levels, and a possible constraining effect of the 0º layer on the cross-ply laminate may exist.

Table 6 presents the θ_d measurements divided in sub-ranges (detailing their percentage of appearance) for both laminates.

As can be observed in Table 6, there is in general a prevalence of large extensions of the interface crack for both types of coupons; in particular, θ_d is commonly higher than 100º. In any case it is necessary to remember the measurement criterion employed which tends to overestimate the results. Thus, for instance, using a ~20º margin, values within the 90°-100° range would lead to values in the 70°-80° one. These new measurements would be in better accordance with the numerical predictions since Correa et al. [1-4] established (for the particular bi-material system employed in their works) a final extension of the crack at the interface θ_d equal to 76º (associated with a crack that extends from 130º to 206º, see Figure 1a).

Notice in any case that the study settled by Correa et al. [1-4] is carried out on the base of a single fibre model, which means an unavoidable difference with the experimental reality of the material here employed (66% fibre content). No isolated fibres with interface cracks have been found in the microscopical inspections here presented, but a second analysis has been performed selecting only the cases in which the fibre is partially isolated or the extension of the crack corresponding to this fibre is perfectly discernible (and thus the measurement criterion is assumed to be free of relevant errors). In order to illustrate this fact, Figure 12 shows an example of several θ_d measurements carried out on different fibres, encircling the one considered as partially isolated (~76.5º).

The selection of debonds corresponding to partially isolated fibres considerably reduces the size of the measurement group, so that the number of measurements is now equal to 24 for the unidirectional case and 50 in the cross-ply group. Notice the difficulty in finding partially isolated fibres in real laminates with high fibre volume content. Table 7 presents the θ_d measurements divided in sub-ranges (in percentage of

appearance) for both groups of samples. From the results it can be deduced now that the amplitudes in the 70º-80º range (those predicted by the numerical results) prevail for both groups of specimens, in agreement with Correa et al. [1,2].

4.5 Measurement of the kinking angle

As it was explained in Section 1, the orientation of the failure plane in coupons tested under transverse compression is commonly around 53º-55º. The numerical studies performed by Correa et al. [1-4] using single-fibre models showed that the numerically predicted kinking angle of the crack into the matrix (Stage III, Figure 1c) coincided with this experimental angle, thus showing a connection between the micro-numerical level and the macro-experimental level. Specifically, and in accordance with a Maximum Circumferential Stress criterion (Erdogan and Sih [21]), it was deducted that the preferential kinking angle was 53º and, by means of an Energy Release Rate study of the kinked crack in the matrix and making use of an energetic criterion (He and Hutchinson [22]), it was demonstrated that 53º was again preferential but standing out only slightly among the rest of the angles in the range of 50º-62º (for the carbon-epoxy system).

At this point it seems crucial to check if the experimental observations carried out in this work allow connecting the numerical and experimental approaches at micro-mechanical level.

With this aim in mind, measurements of the kinking angle in macro-cracks of coupons tested until breakage have been performed. A predominant range of 50º-60º arises (in agreement with [3]) although kinking angles outside this range were also

measured. Moreover, many examples of cracks that kink into the matrix following an orientation between 53º and 55º have been found, which, in fact is the prevailing sub-range within the aforementioned 50º-60º range. Figure 13 demonstrates this fact as shown in the picture (corresponding to a unidirectional coupon) from an interface crack kinking into the matrix following an orientation of ~54.5º.

5. Conclusions

This work focused on the experimental identification of the different stages of the inter-fibre failure under compression in carbon-epoxy coupons.

Tests and microscopical inspection on coupons from 90º unidirectional and $[0_3,90_3]$s laminates allowed the following conclusions to be established:

- No macro-cracks, visible at low magnification, were detected in the unidirectional and cross-ply coupons before final failure. Instead, some macro-cracks were identified in both types of coupons at loading levels close to breakage using high magnification.
- In both types of coupons the microscopical inspection revealed the presence of the different stages of damage progression predicted numerically in previous works [1-3].
- The measurement of the interface crack length that gives rise to interface cracks kinking towards the matrix (Stage III) showed that the preferential debonding angle is in the range of 70º-80º, reasonably matching previous numerical predictions.

- No fibre-matrix debonds smaller than 20º were found, suggesting this is the minimum debond length at the onset of fibre-matrix interface cracking, at least for the material system studied in the present work.
- Kinking angles in the preferential range 50º-60º were found experimentally, confirming the numerical predictions presented in [3].

It is noted that the work presented here validates, to a large extent, the previous numerical predictions by the authors.

Finally, to complement this work, scanning electronic microscopy could be used to study aspects such as Stage I identification in depth, and even interesting features that have not been studied in this investigation such as the morphology of the interface crack (in particular, the contact zone at the upper crack tip and the 'bubble' at the lower crack tip [1]) and the longitudinal growth of the crack along the 1-axis (i.e. crack tunneling) as it grows circumferentially.

Acknowledgements

This work was supported by the Spanish Ministry of Education, Culture and Sports under Grants MAT2016-80879-P and MAT2013-45069-P.

References

[1] Correa E, París F, Mantič V. Numerical characterisation of the fibre-matrix interface crack growth in composites under transverse compression. Eng Fract Mech 2008;75:4085-4103.

[2] Correa E, París F, Mantič V. A micromechanical view of inter-fibre failure of composite materials under compression transverse to the fibres. Compos Sci Technol 2008;68:2010-2021.

[3] Correa E, París F, Mantič V. BEM analysis of inter-fibre failure under compression in composites: comparison between carbon and glass fibre systems. Plast Rubber Compos 2011;40(6/7):333-341.

[4] Correa E, París F, Mantič V. Effect of thermal residual stresses on the matrix failure under transverse compression at micromechanical level – a numerical and experimental study. Compos Part A – Appl Sci Manuf 2012;43:87-94.

[5] González C, Llorca J. Mechanical behaviour of unidirectional fiber-reinforced polymers under transverse compression: microscopic mechanisms and modeling. Compos Sci Technol 2007;67(13):2795-2806.

[6] Vaughan TJ, McCarthy CT. Micromechanical modelling of the transverse damage behaviour in fibre reinforced composites. Compos Sci Technol 2011;71(3):388-396.

[7] Lei Yang, Ying Yan, Yujia Liu, Zhiguo Ran. Microscopic failure mechanisms of fiber-reinforced polymer composites under transverse tension and compression. Compos Sci Technol 2012;72(15):1818-1825.

[8] Arteiro A, Catalanotti G, Melro AR, Linde P, Camanho PP. Micro-mechanical analysis of the effect of ply thickness on the transverse compressive strength of polymer composites. Compos Part A – Appl Sci Manuf 2015;79:127-137.

[9] Puck A, Schürmann H. Failure analysis of FRP laminates by means of physically based phenomenological models. Compos Sci Technol 1998;58(7):1045-1067.

[10] Christensen RM, de Teresa SJ. Failure plane orientations for transverse loading of a unidirectional fiber composite. Int J Solids 2003;40(25):7055-7062.

[11] Zhang H, Ericson ML, Varna J, Berglund LA. Transverse single-fibre test for interfacial debonding in composites: 1. Experimental observation. Compos Part A – Appl Sci Manuf 1997;28(4):309-315.

[12] Gamstedt EK, Sjögren BA. Micromechanisms in tension-compression fatigue of composite laminates containing transverse plies. Compos Sci Technol 1999;59(2):167-178.

[13] Saito H, Takeuchi H, Kimpara I. Experimental evaluation of the damage growth restraining in 90° layers of thin-ply CFRP cross-ply laminates. Adv Compos Mater 2012;21(1):57-66.

[14] Baral N, Guezenoc H, Davies P, Baley C. High modulus carbon fibre composites: Correlation between transverse tensile and mode I interlaminar fracture properties. Materials Letters 2008;62(6-7):1096-1099.

[15] Hobbiebrunken T, Hojo M, Adachi T, Jong CD, Fiedler B. Evaluation of interfacial strength in CF/epoxies using FEM and in-situ experiments. Compos Part A – Appl Sci Manuf 2006;37(12):2248-2256.

[16] Genz M, Armentrout D, Rupnowski P, Kumosa L, Shin E, Sutter J, Kumosa M. In-plane shear testing of medium and high modulus woven graphite fiber reinforced/polyimide composites. Compos Sci Technol 2004;64(2):203-220.

[17] ASTM D695-02a. Standard Test Method for Compressive Properties of Rigid Plastics, ASTM International, West Conshohocken, PA, 2003.

[18] Correa E, Valverde M, Velasco ML, París F. Microscopical observations of inter-fibre failure under tension. Compos Sci Technol 2018;155:213-220.

[19] Mantič V. Interface crack onset at a circular cylindrical inclusion under a remote transverse tension. Application of a coupled stress and energy criterion. Int J Solids 2009;46(6):1287-1304.

[20] Mantič V, García IG. Crack onset and growth at the fibre-matrix interface under a remote biaxial transverse load. Application of a coupled stress and energy criterion Int J Solids. 2012;49(17):2273-2290.

[21] Erdogan F, Sih GC. On the crack extension in plates under plane loading and transverse shears. J Basic Eng 1963;85:519-27.

[22] He MY, Hutchinson JW. Kinking of a crack out of an interface. J Appl Mech 1989;56:270-278.

Figure 1. Stages of the inter-fibre failure under compression (Correa et al. [2]).

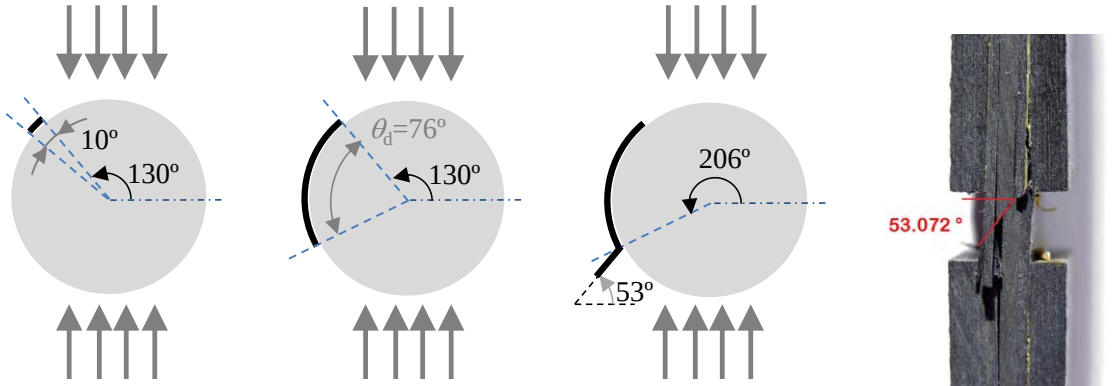

a) Stage I b) Stage II c) Stage III d) Macro-failure

Figure 2. Coupons geometry (dimensions in mm).

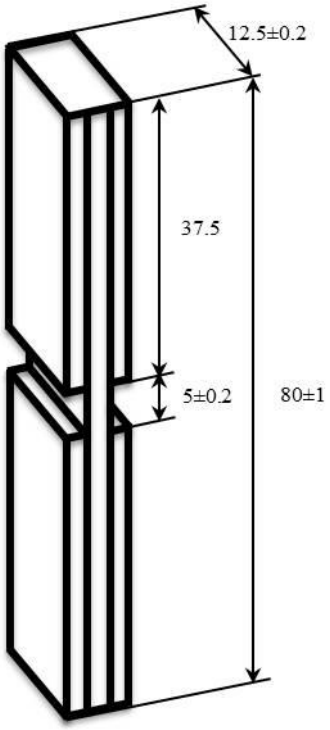

Figure 3. (a) Unidirectional coupon, (b) cross-ply coupon.

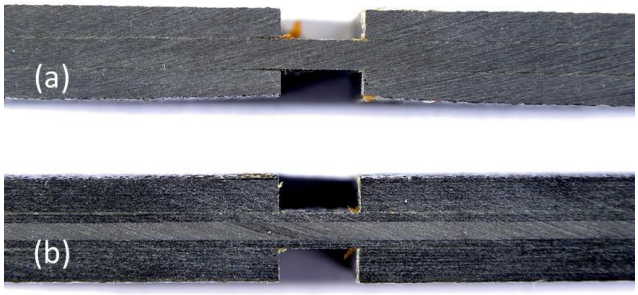

Figure 4. Compressive test set-up.

Figure 5. (a) Diamond disc (MD-Dac), (b) lubrication with DiaPro Dac 3 μm liquid, (c) polishing.

(a) (b) (c)

Figure 6. Sample (a) before polishing (b) after polishing.

(a) (b)

Figure 7. (a) Stage I (UD coupon, 25%Y_c), (b) Stage II (UD coupon, 50%Y_c), (c) Stage III (UD coupon, 50%Y_c), (d) Stage IV (UD coupon, 100%Y_c).

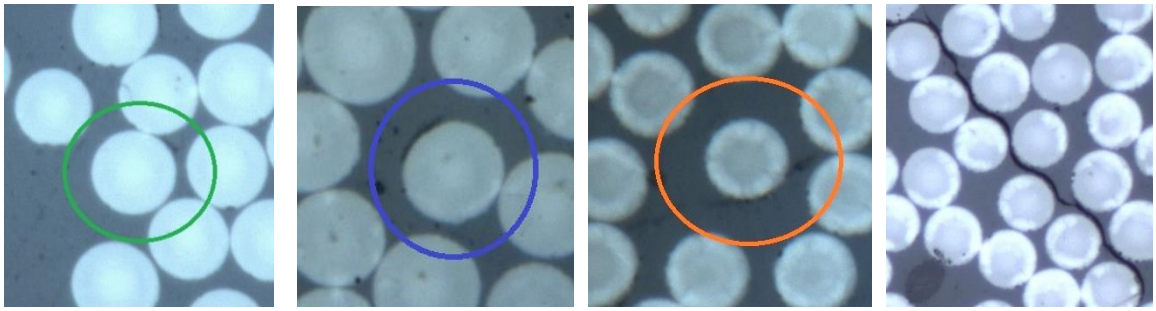

(a) (b) (c) (d)

Figure 8. Other types of damage: (a) Hole (UD coupon, 75%Y_c), (b) tangent crack (UD coupon, 25%Y_c), (c) crack touching a fibre (UD coupon, 25%Y_c), (d) matrix crack (UD coupon, 50%Y_c).

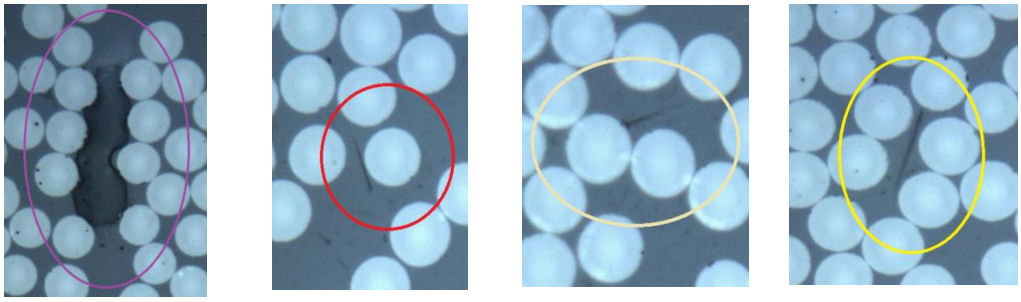

(a) (b) (c) (d)

Figure 9. Very large debond.

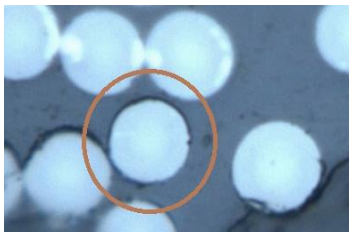

Figure 10. Measurement of a debond corresponding to Stage I.

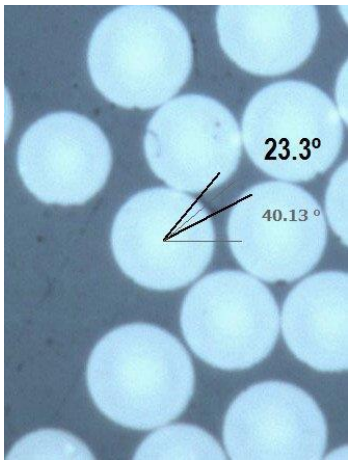

Figure 11. Explanation on the criterion selected for measuring interface cracks.

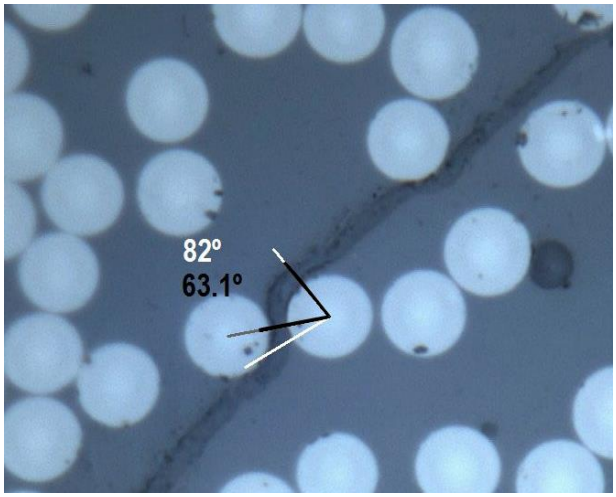

Figure 12. θ_d measures in partially isolated and non-isolated fibres.

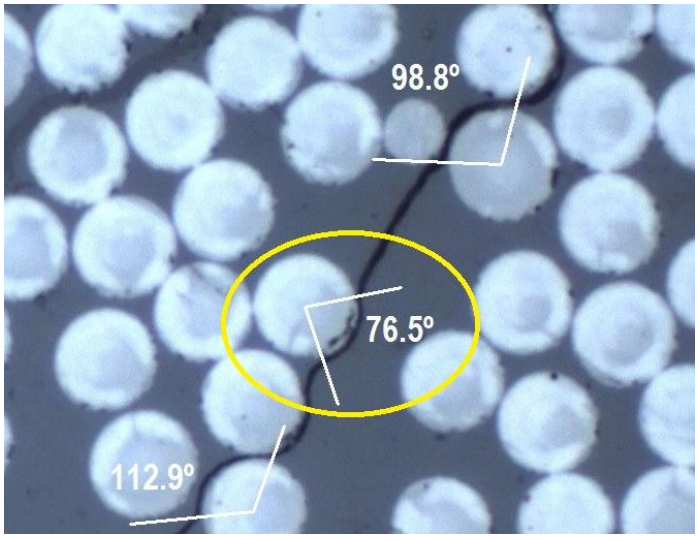

Figure 13. Measurement of the kinking angle.

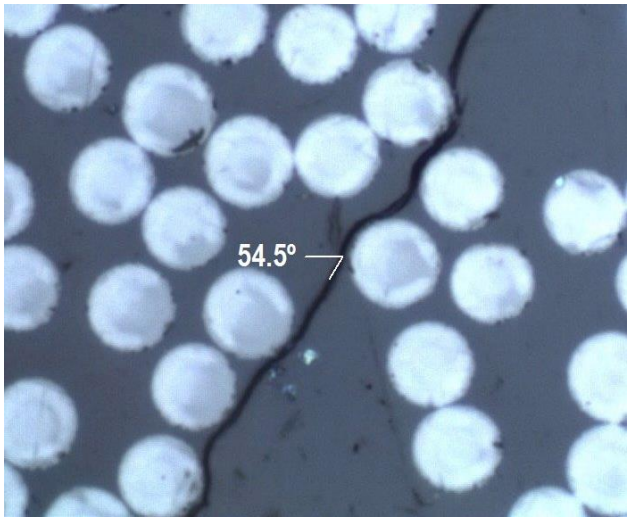

Table 1. Steps of the polishing process.

Step	Disc	Liquid	Pressure	Speed	Time
1	*SiC #320* µm	Water	40 N	80 rpm	5’
2	*MD-Largo*	*DiaPro Allegro/Largo 9 µm*	40 N	80 rpm	6’
3	*MD-Dac*	*DiaPro Dac 3 µm*	40 N	80 rpm	5’
4	*MD-Nap*	*DiaPro Nap B1 1 µm*	40 N	80 rpm	3’

Table 2. Number of inspected imperfections (unidirectional coupons).

	25%Y_c	50%Y_c	75%Y_c	80%Y_c
Number of imperfections	182	130	66	117

Table 3. Imperfections occurrence (unidirectional coupons).

	25%Y_c	50%Y_c	75%Y_c	80%Y_c
Stage I	4.9%	2.3%	1.5%	0.8%
Stage II	2.7%	4.6%	3%	2.6%
Stage III	1.7%	3.1%	1.5%	4.3%
Stage IV	0%	1.5%	0%	1.7%
Damage V	4.4%	3.1%	24.3%	12.8%
Damage VI	34.1%	44.6%	36.4%	34.2%
Damage VII	13.7%	10.8%	1.5%	11.1%
Damage VIII	38.5%	30%	31.8%	32.5%

Table 4. Number of inspected imperfections (cross-ply coupons).

	70%X	75%X	90%X	95%X	95%X (b)
Number of imperfections	49	17	100	116	296

Table 5. Imperfections occurrence (cross-ply coupons).

	70%X	75%X	90%X	95%X	95%X (b)
Stage I	0%	0%	0%	0%	2.3%
Stage II	4.1%	0%	4%	6%	5.8%
Stage III	6.1%	5.9%	0%	4.3%	5%
Stage IV	0%	0%	3%	7.8%	0.7%
Damage V	16.3%	23.5%	29%	13.8%	10.5%
Damage VI	28.6%	11.8%	32%	30.2%	42.9%
Damage VII	0%	0%	0%	8.6%	9.5%
Damage VIII	44.9%	58.8%	32%	29.3%	23.3%

Table 6. θ_d distribution and percentage of appearance.

θ_d	90_{10}	$[0_3, 90_3]_s$
<60°	10.9%	12.5%
60°-70°	13.3%	11.0%
70°-80°	22.1%	16.4%
80°-90°	17.1%	16.7%
90°-100°	12.1%	11.7%
>100°	24.5%	31.7%

Table 7. θ_d distribution and percentage of appearance in partially isolated fibres.

θ_d	90_{10}	$[0_3, 90_3]_s$
<60°	29.2%	18.0%
60°-70°	8.3%	10.0%
70°-80°	33.3%	26.0%
80°-90°	16.7%	12.0%
90°-100°	12.5%	10.0%
>100°	0%	24.0%